

An electrochemical investigation on (MoO_3 +PVP+PVA) nanobelts for lithium batteries

Ch. V. Subba Reddy · Y. Y. Qi · W. Jin · Q. Y. Zhu ·
Z. R. Deng · W. Chen · Sun-il Mho

Received: 17 October 2006 / Revised: 7 January 2007 / Accepted: 12 January 2007 / Published online: 15 February 2007
© Springer-Verlag 2007

Abstract Molybdenum trioxide (MoO_3) xerogel films modified with poly(vinyl alcohol)+poly(vinyl pyrrolidone) (PVP+PVA) polyblends were obtained by ion-exchange method with sol-gel technique. Investigations were conducted using X-ray “diffractometry”, Fourier transform infrared spectroscopy, and cyclic voltammetry. The results show that the H atoms in polyblend are H-bonded with the O atoms in the Mo=O bonds of MoO_3 xerogel, which effectively shield the electrostatic interaction between MoO_3 interlayer and Li^+ ions when MoO_3 xerogel is modified by the intercalation of (PVP+PVA). The reversibility of the insertion/extraction of Li^+ ions is greatly improved by the modification with polyblend of MoO_3 nanocomposite films. MoO_3 and $(\text{PVP+PVA})_x\text{MoO}_3$ ($x=0, 0.5$) nanobelts were obtained by a simple hydrothermal process from MoO_3 sol. The electrochemical cells with configuration $\text{Li}/(\text{LiPF}_6+\text{EC+DMC})/\text{MoO}_3$ modified by (PVP+PVA) were fabricated and their discharge profiles studied.

Keywords Polymer · MoO_3 nanobelts · XRD · FTIR · Lithium battery

Introduction

The increasing demand for small-size autonomous power sources raises the interest in thin-layer lithium batteries [1, 2]. Comparatively, the inexpensive trioxide MoO_3 has a high primary discharge capacity but a lower discharge voltage as compared with V_2O_5 and MnO_2 [3]. Nevertheless, lithium batteries based on MoO_3 are competitive among other lithium batteries with solid-phase cathodes. A number of small-sized Li– MoO_3 batteries are already produced industrially [4]. Its theoretical Li insertion capacity is difficult to attain in practice due to irreversible phase transformation in the crystalline form or irreversible Li insertion in the case of the xerogel [5]. Many researchers have modified MoO_3 with polymer, such as poly(*p*-phenylene vinylene) (PPV), poly-aniline (PAN), or nylon, poly(ethylene-oxide) (PEO) [6–9], but modifying MoO_3 xerogel with poly(vinyl alcohol)+poly(vinyl pyrrolidone) (PVP+PVA) has not been reported. The intercalation of PVP/PVA is expected to enhance the mobility of Li^+ ions in MoO_3 xerogel interlayer and improve the reversibility of insertion/extraction of Li^+ ions. The preparation of modified MoO_3 xerogel film and the effect of modification by PVP/PVA on the reversibility of insertion/extraction of Li^+ ion in MoO_3 nanocomposite films are investigated and discussed, and the electrochemical property of MoO_3 nanobelts were reported in this paper.

Experimental

A clear light-blue MoO_3 sol.(pH 2.0) was prepared by an ion exchange of $(\text{NH}_4)_6\text{Mo}_7\text{O}_{24}\cdot 4\text{H}_2\text{O}$ ($\geq 99.0\%$) through a proton exchange resin of particle size 0.3–1.2 mm (from a Shanghai agent company). The PVP+PVA (50:50) was dissolved in distilled water, and the solution was mixed

C. V. Subba Reddy · Y. Y. Qi · W. Jin · Q. Y. Zhu · Z. R. Deng ·
W. Chen (✉)

Institute of Materials Science and Engineering,
Wuhan University of Technology,
Wuhan 430-070, China
e-mail: chenw@mail.whut.edu.cn

C. V. Subba Reddy
e-mail: subbu5reddy@yahoo.co.in

C. V. Subba Reddy · S.-i. Mho
Division of Energy Systems Research, Ajou University,
Suwon 443-749, South Korea

with MoO_3 sol. The molar ratio of polyblend to MoO_3 was x : 1 ($x=0, 0.5$). The composite membrane was formed in glass substrate by dip-coating method after the mixed sol was left motionless for 2 or 3 days. The MoO_3 and $(\text{MoO}_3+\text{PVP}+\text{PVA})$ xerogel films were produced by heating the composite membranes for 36 h at 373 K under vacuum.

The MoO_3 and $(\text{MoO}_3+\text{PVP}+\text{PVA})$ nanobelts from their sols were synthesized by a hydrothermal process. The mixed solutions were directly added into Teflon-lined autoclaves and kept at 180 °C for 4 days. After the hydrothermal reaction, the light blue product was washed with distilled water and ethanol and dried at 80 °C for 8 h. Oxygen post-treatment was carried out by heating the as-prepared $(\text{MoO}_3+\text{PVP}+\text{PVA})$ nanoparticles at 100 °C for 3 h under a constant oxygen flow in a furnace.

The X-ray diffraction (XRD) patterns of the films were measured with HZG4/B-propylene carbonate (PC) X-ray diffractometer with $\text{CoK}\alpha$ radiation and graphite “monochromator.” Fourier transform infrared (FTIR) absorption spectra of the films were recorded using a 60-SXB IR spectrometer with a resolution of 4 cm^{-1} , over a range of 400–4,000 cm^{-1} . Employing the JSM-5610LV scanning electron microscope, SEM images were collected. The cyclic voltammogram (CV) was performed with scan rate of 1 mV/s by electrochemical method in a non-aqueous lithium cell using 1 M LiClO_4 dissolved in PC electrolyte. The electrochemical cell was a standard three-electrode system. Indium tin oxide conducting glass coated with the modified MoO_3 xerogel film and platinum foil was used as a working electrode and as well as counter electrode. A standard calomel electrode was used as a reference electrode. The electrochemical characteristic study was carried out using a multichannel galvanostat/potentiostat system (MacPile). In the prepared electrochemical cells, a lithium pellet was used as negative electrode, a 1 mol dm^{-3} solution of LiPF_6 in ethylene carbonate/dimethyl carbonate as electrolyte, and a pellet made of the MoO_3 , $(\text{MoO}_3+\text{PVP}+\text{PVA})$ nanobelts, acetylene black and polytetrafluoroethylene in a 85:10:05 ratio, as the positive electrode.

Results and discussion

XRD analysis

The XRD patterns of MoO_3 xerogel both before and after modification with PVP/PVA are shown in Fig. 1. The XRD pattern of MoO_3 xerogel shows three peaks whose d values are 0.692, 0.347, and 0.234 nm corresponding to the diffraction of (020), (040), and (060) crystal planes, respectively [10]. No (hol) or (hkl) reflections are observed in Fig. 1, confirming the turbostratic nature of the MoO_3 slabs perpendicular to the b -direction axis. The repeated

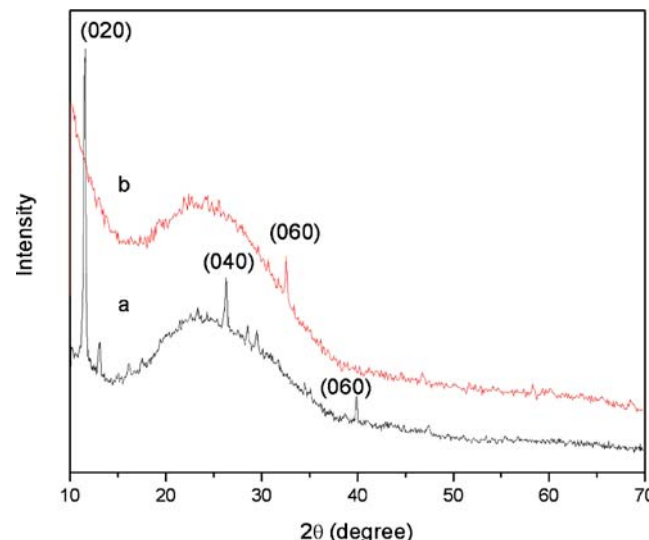


Fig. 1 XRD patterns of (a) MoO_3 xerogel (b) MoO_3 intercalated with (PVP+PVA)

distance in the modified MoO_3 xerogel film increases from 0.234 nm to 0.284 nm for MoO_3 xerogel film modified by PVP/PVA in which peaks of (020) and (040) crystal planes vanish. The increase in repeated distance is because PVP/PVA intercalates in MoO_3 xerogel interlayer and opens the MoO_3 xerogel layers [11, 12]. The disappearance of some peaks shows the reduction of the crystalline arrangement in the b -direction with the modification with PVP/PVA intercalating in the interlayer [13].

The XRD patterns of the polyblend intercalated $(\text{PVP}+\text{PVA})_x\text{MoO}_3$ ($x=0, 0.5$) nanobelts are shown in Fig. 2. All the diffraction peaks can be indexed to the MoO_3 phase consistent with the standard value of JCPDS no.05-0508. The strong intensity of reflection peaks of (020), (040), and (060) indicate the anisotropic growth. The diffraction peaks (020), (110), (040), (021), and (060) of the polyblend inter-

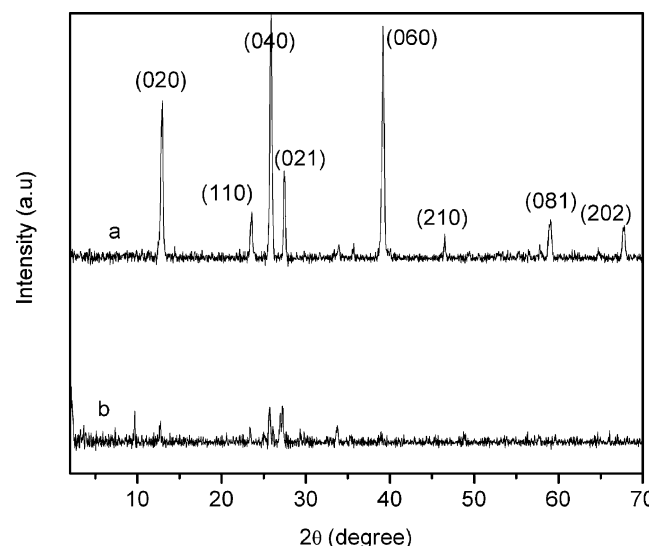


Fig. 2 XRD spectra of (a) MoO_3 , (b) $(\text{PVP}+\text{PVA})_{0.5}\text{MoO}_3$ nanobelts

calated $(\text{PVP+PVA})_x\text{MoO}_3$ ($x=0.5$) nanobelts are shifted lower angle side, and (210), (081), and (202) have disappeared. The diffraction peak shifts indicate the increasing distance between the interlayer of MoO_3 . The disappearance of some the peaks indicates the increasing amorphousness in the MoO_3 interlayer.

FTIR spectrum analyses

FTIR spectra of MoO_3 xerogel both before and after the modification with PVP/PVA are shown in Fig. 3. The MoO_3 xerogel exhibits three main vibration modes in the 400–4,000 cm^{-1} range. The terminal oxygen symmetry stretching mode (ν_s) of $\text{Mo}=\text{O}$, the bridge oxygen asymmetry, and symmetry stretching modes (ν_{as} and ν_s) of $\text{Mo}-\text{O}-\text{Mo}$ are at 999, 870, and 567 cm^{-1} , respectively [5]. FTIR spectra of MoO_3 xerogel intercalated by (PVP+PVA) shows the characteristic intense peaks at 1,292 and 1,401 cm^{-1} , which indicates the presence of (PVP+PVA), and small and poorly resolved peak at 2,919 cm^{-1} is an indication of amorphous (PVP+PVA) phase, which is different from that of crystalline (PVP+PVA) [14]. A remarkable change in vibration modes and peak shifts to lower wave numbers were noticed in the (PVP+PVA) intercalated MoO_3 xerogel. The ν_s ($\text{Mo}=\text{O}$) shits from 999 to 988 cm^{-1} , which indicates that the $\text{Mo}=\text{O}\cdots\text{H}$ bond is formed in the nanocomposite materials [15]. Namely, the H atoms in the (PVP+PVA) are H-bonded with the O atoms in the $\text{Mo}=\text{O}$ bonds of MoO_3 xerogel.

CV analyses

Figure 4 shows the CV curves of MoO_3 xerogel both before and after modification with PVP/PVA. The measured scan

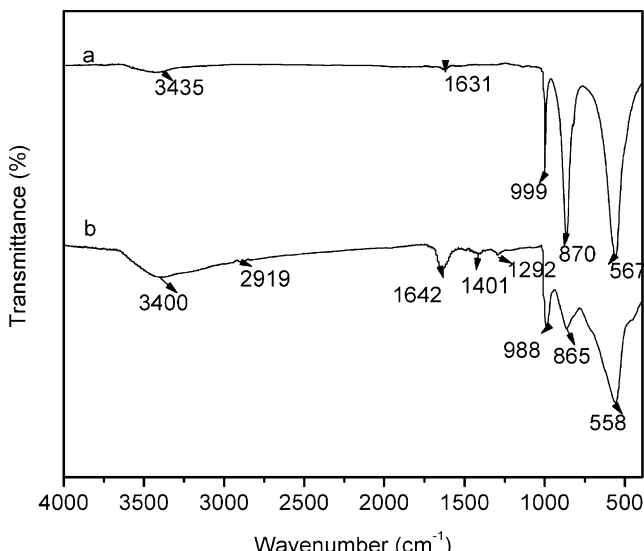


Fig. 3 FTIR spectra of (a) $\text{Mo}_3\text{O}_2\text{S}$ xerogel and (b) $\text{Mo}_3\text{O}_2\text{S}$ intercalated with (PVP+PVA)

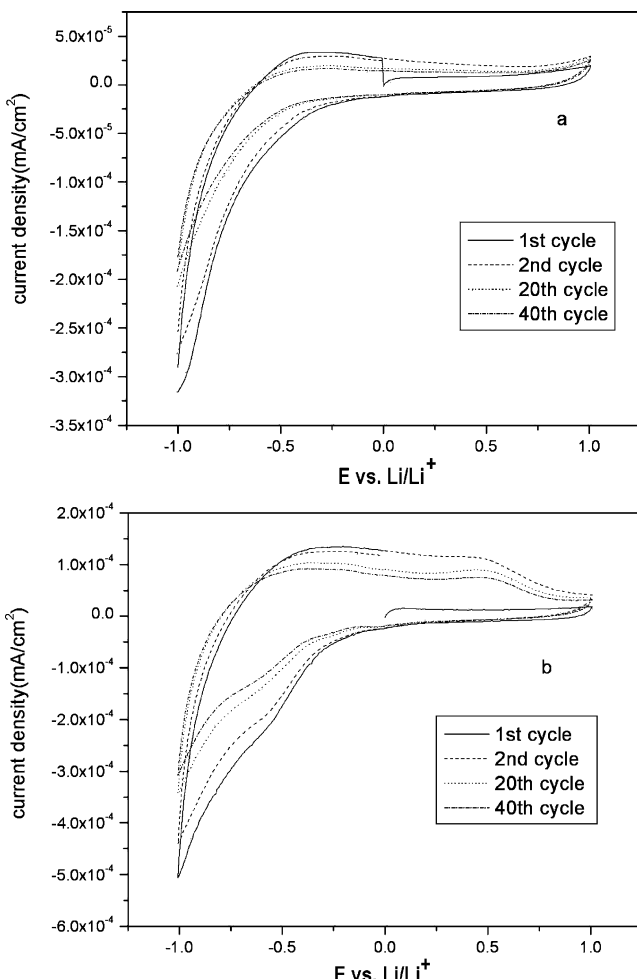


Fig. 4 Cyclic voltammetric curves of **a** $\text{Mo}_3\text{O}_2\text{S}$ xerogel and **b** $\text{Mo}_3\text{O}_2\text{S}$ intercalated with (PVP+PVA) sol-gel films measured at a scan rate of 1 mV/s

rate is of 1 mV/s in which the 1st, 2nd, 20th, and 40th cycle curves were plotted. The curve area (A_i) surrounded by each cycle represents the amount of Li^+ ion insertion. The cycle efficiency is calculated by the following equation:

$$Q_i = A_i/A_1$$

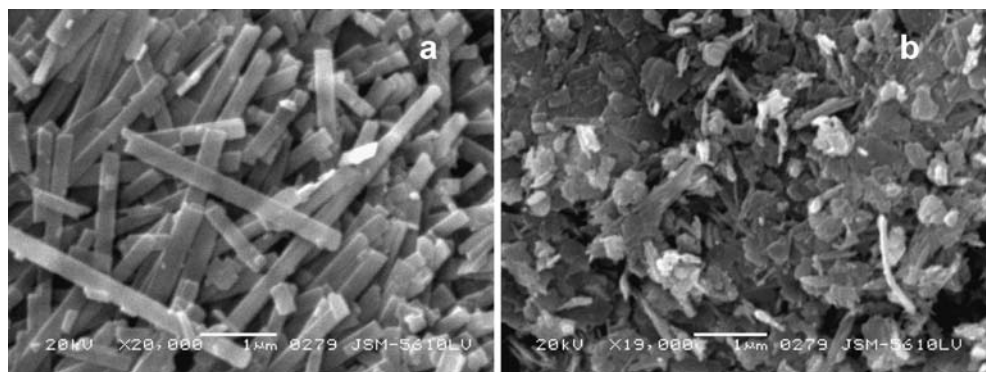
where Q_i is the cycle efficiency, A_1 is the area of the first cycle curve and A_i is the area of the i th cycle curve. The cycle efficiencies of different cycle times and compositions are listed in Table 1.

The calculated second cycle efficiency (Q_2) of the $\text{Mo}_3\text{O}_2\text{S}$ and PVP+PVA intercalated $\text{Mo}_3\text{O}_2\text{S}$ xerogels are 88.23 and

Table 1 The cycle efficiency of different cycle times and compositions

Sample	Q_2 (%)	Q_{20} (%)	Q_{40} (%)
$\text{Mo}_3\text{O}_2\text{S}$ xerogel	88.23	63.17	46.51
$\text{Mo}_3\text{O}_2\text{S}$ xerogel intercalated with PVP+PVA	76.85	70.25	51.25

Fig. 5 SEM photographs of **a** MoO₃ nanobelts and **b** MoO₃ nanobelts intercalated with (PVP+PVA)



76.85%, respectively. In the modified film, the Q_2 is lowered because a portion of Li⁺ ions complexed by PVP/PVA chains cannot be extracted from the interlayer. The cycle efficiencies Q_{20} and Q_{40} of PVP+PVA intercalated MoO₃ xerogel films are 70.25 and 51.25%. These are higher than that of MoO₃ xerogel film (63.17 and 46.51%), which indicates that the cycling stability tends to increase after several cycles. The Q_{20} of MoO₃ xerogel film before intercalation with PVP/PVA apparently decreases from 88.23 to 63.17%, primarily owing to the strong electrostatic interactions between Li⁺ ions and oxygen atoms of the MoO₃ lattice. When (PVP+PVA) is intercalated into MoO₃ xerogel, it has relatively strong interactions with MoO₃ layers and a complexing interaction with Li⁺ ions, which is effectively shielding electrostatic interactions between Li⁺ ions and MoO₃ [16]. As a result, the cycling stability has improved and the reversibility of the insertion/ extraction of Li⁺ ions in the MoO₃ interlayer enhanced.

SEM analyses

Morphological effects are responsible for improved electrochemical activities [17]. Figure 5a shows the SEM image of the MoO₃ nanobelts exhibiting a wide range of widths ranging from 100 to 600 nm. The lengths of nanobelts are in the order of 1–6 μm. The nanobelts are straight and have rectangular flat tips with four sharp corners at the upper ends. Smooth facets enclose the surfaces of the nanobelts and from the sharp edges. Figure 5b shows the SEM image of the (PVA+PVA) intercalated MoO₃ xerogel. Ultrafine spherical particles of molybdenum trioxide with the diameter of 100 to 800 nm are observed.

Electrochemical characteristics

Figure 6 shows the first discharge curves of (a) as-prepared MoO₃ nanobelts, (b) modified MoO₃+PVP+PVA nanobelts, and (c) post-oxygen-treated MoO₃+PVP+PVA nanobelts. The measured specific discharge capacitance of the as-prepared MoO₃ nanobelts battery in the potential range of

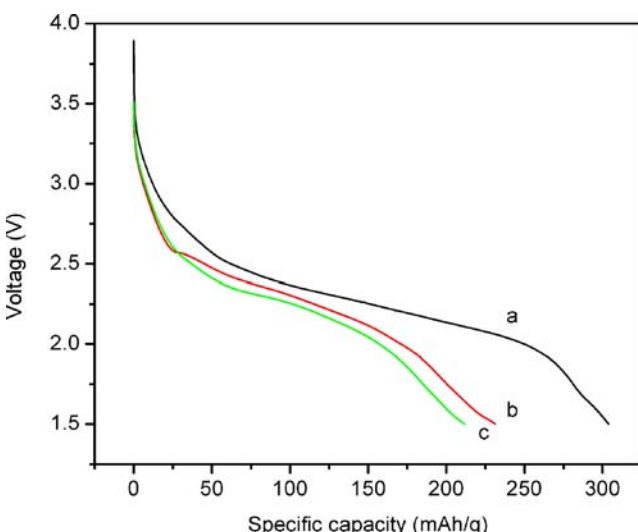


Fig. 6 First discharge curves of (a) MoO₃ nanobelts, (b) pre-post-oxygen-treated (MoO₃+PVP+PVA), and (c) post-oxygen-treated (MoO₃+PVP+PVA) nanobelts secondary batteries

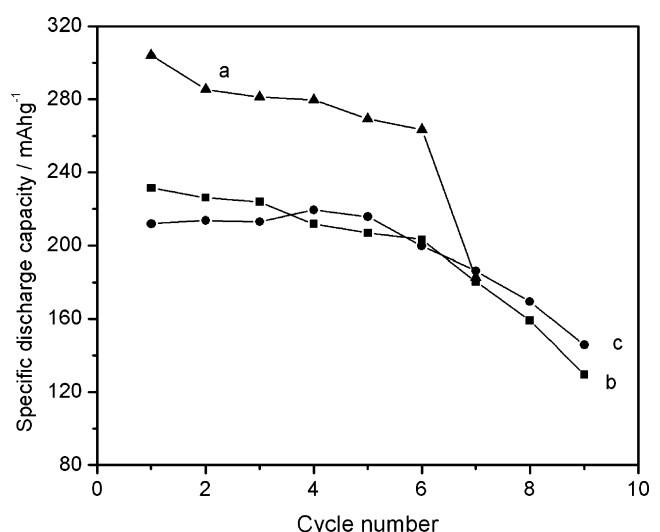


Fig. 7 Cycling property of (a) MoO₃ nanobelts, (b) pre-post-oxygen treated (MoO₃+PVP+PVA), and (c) post-oxygen-treated (MoO₃+PVP+PVA) nanobelts secondary batteries

3.85–1.5 V is 303 mAh/g, and (MoO₃+PVP+PVA) nanobelts and post-oxygen-treated (MoO₃+PVP+PVA) nanobelts batteries measured in the potential range of 3.45–1.5 V are 231 and 211 mAh/g, respectively. The decrement in the specific discharge capacities in the modified and post-oxygen-treated nanobelt batteries might be due to a decreased average molybdenum oxidation state as a result of the intercalation of polymers towards lithium insertion. Figure 7 shows nine complete charge–discharge cycles of the battery. The specific discharge capacity is 263 mAh/g after six cycles of the MoO₃ nanobelts, and cell exhibits a capacity loss of only 14%; after seven cycles, the capacity loss is 40%, which indicates the poor Faradic efficiency of both electrodes. The specific discharge capacity of the (MoO₃+PVP+PVA) battery after nine cycles is 155 mAh/g, exhibits a capacity loss of 33%. The specific discharge capacity of post-oxygen-treated (MoO₃+PVP+PVA) battery after nine cycles is 165 mAh/g and exhibits a capacity loss of 22%, which indicates that the post-oxygen-treated battery has more stable reversible electrochemical performance. In the polymer-intercalated samples, post oxygen treatment plays a role in activating polymer as an electrochemical active species for lithium insertion. Similarly, the effect of oxygen treatment has been observed for PANI/V₂O₅, [18, 19] and PPy/V₂O₅ [20, 21]. The improved cycle stability by post oxygen treatment is probably due to the partially re-oxidized MoO₃ oxidation states, and polymer chains inside the MoO₃ gallery couple oxidatively from longer chains [22].

Conclusions

PVP/PVA has been intercalated into MoO₃ xerogels. The intercalation is confirmed by XRD, FT-IR, and CV. The results show that the H atoms in PVP+PVA are H-bonded with the O atoms of the Mo=O bonds of MoO₃ xerogel, which effectively shields the electrostatic interaction between MoO₃ interlayer and Li⁺ ions when MoO₃ xerogel is intercalated with PVP+PVA. The as-prepared (PVP+PVA)/MoO₃ exhibits a slightly lower discharge capacity than the pure MoO₃. After oxygen post treatment of the (PVP+

PVA)/MoO₃, batteries exhibit more cycle stability than the pure MoO₃ nanobelts battery.

Acknowledgment One of the authors (Ch. V. S. Reddy) thanks Wuhan University of Technology for his Post Doctoral Fellowship award, and he also thanks Ajou University for his Post Doctoral Fellowship award from the BK 21 project. Authors thank Dr. Rajamohan R Kalluru, Mississippi Ethanol LLC, USA for fruitful discussions.

References

1. Dampier F (1974) J Electrochem Soc 121:121
2. Margalit N (1974) J Electrochem Soc 121:1460
3. Kumagai N, Tanno K (1987) J Electrochem Soc 134:406
4. Nijnikovsky E (1998) J Electrochem Soc 34:772
5. Leroux F, Koene BE, Nazar LF (1997) J Electrochem Soc 144:3886
6. Nazar LF, Zhang Z, Zinkweg D (1992) J Am Chem Soc 114:6239
7. Posudievsky OY, Biskulova SA, Pokhodenko VD (2002) J Mater Chem 12:1446
8. Wang L, Schindler J, Kannewurf CR (1997) J Mater Chem 7:1277
9. Hu Y, Chen W, Xu Q (2001) J Mater Sci Technol 17:124
10. Chen W, Xu Q, Yuan RZ (2000) Mater Sci Eng B 77:15
11. Anassis FJ, Demets GJF, Toma HE (1999) Electrochim Commun 1:332
12. Tetsuoldzu SK, Martin CR, Yoneyama H (1998) J Electrochem Soc 145:2707
13. Ramana CV, Hussain OM, Naidu BS (1997) Mater Chem Phys 50:195
14. Harrel J, Wong HP, Dave BC, Dunn B, Nazar LF (1998) J Non-cryst Solids 225:319
15. Chen W (1998) Synthesis, structure and properties of polymer-layered silicate nanocomposite, D.S. Dissertation, Wuhan University of Technology, p 6
16. Chen W, Xu Q, Hu YS, Mai LQ, Zhu QY (2002) J Mater Chem 12:1926
17. Pringle JM, Forsyth M (2004) Polymer 45:1447
18. Leroux F, Koene BE, Nazar LF (1996) J Electrochem Soc 143: L181
19. Lira-Cantu M, Gomez-Romero P (1999) J Electrochem Soc 146:2029
20. Wong HP, Dave BC, Leroux F, Harrel J, Dunn B, Nazar LF (1998) J Mater Chem 8:1019
21. Goward G, Leroux F, Nazar LF (1998) Electrochim Acta 43:1307
22. Wu CG, De Groot DC, Marcy HQ, Schindler JL, Kannewurf CR, Liu YJ, Hirpo W, Kanatzidis MG (1996) Chem Mater 8:1992